

VILNIUS UNIVERSITY

Rimtautas Piskarskas

**SPATIO-TEMPORAL CHARACTERIZATION OF  
PROPAGATION OF INTENSE FEMTOSECOND LIGHT  
WAVE PACKETS IN KERR MEDIA**

Summary of doctoral thesis

Physical sciences, Physics (02P)

Vilnius, 2009

Doctoral dissertation prepared 2004-2009 at the Department of Quantum electronics of Vilnius University.

Scientific supervisor:

Prof. Dr. (HP) **Audrius Dubietis** (Vilnius University, Physical sciences, Physics – 02P).

Scientific advisor:

Prof. Habil. Dr. **Algirdas Stabinis** (Vilnius University, Physical sciences, Physics – 02P).

Doctoral Dissertation will be defended in the Council of Physics of Vilnius University:

Chairman:

Prof. Habil. Dr. **Valdas Sirutkaitis** (Vilnius University, Physical sciences, Physics – 02P).

Members:

Prof. Dr. (HP) **Gintaras Valiulis** (Vilnius University, Physical sciences, Physics – 02P).

Prof. Habil. Dr. **Valerijus Smilgevičius** (Vilnius University, Physical sciences, Physics – 02P).

Doc. Dr. **Valdas Girdauskas** (Vytautas Magnus University, Physical sciences, Physics – 02P).

Prof. Habil. Dr. **Gintautas Jurgis Babonas** (Semiconductor Physics Institute, Physical sciences, Physics – 02P).

Oponents:

Prof. Habil. Dr. **Arūnas Krotkus** (Semiconductor Physics Institute, Physical sciences, Physics – 02P).

Dr. **Rimantas Grigonis** (Vilnius University, Physical sciences, Physics – 02P).

The official defense of the Dissertation will be held at 3 p.m. on 2 July 2009 in 510<sup>th</sup> auditorium at Physics Department of Vilnius University, Saulėtekio ave. 9, bldg. 3, LT-10222 Vilnius, Lithuania.

Summary of the Doctoral Dissertation has been distributed on 2 June 2009.

The Dissertation is available at the libraries of Vilnius University, Institute of Physics and Martynas Mažvydas National Library Of Lithuania.

VILNIAUS UNIVERSITETAS

Rimtautas Piskarskas

**INTENSYVIŲ FEMTOSEKUNDINIŲ ŠVIESOS BANGŲ  
PAKETŲ SKLIDIMO KERO TERPĖSE LAIKINIS IR  
ERDVINIS CHARAKTERIZAVIMAS**

Daktaro disertacija  
Fiziniai mokslai: fizika (02P)

Vilnius, 2009

Disertacija rengta 2004 – 2009 metais Vilniaus universitete.

Mokslinis vadovas:

Prof. dr. (HP) **Audrius Dubietis** (Vilniaus Universitetas, fiziniai mokslai, fizika – 02P).

Konsultantas:

Prof. habil. dr. **Algirdas Stabinis** (Vilniaus Universitetas, fiziniai mokslai, fizika – 02P).

Disertacija ginama Vilniaus universiteto Fizikos mokslo krypties taryboje:

Pirmininkas:

Prof. habil. dr. **Valdas Sirutkaitis** (Vilniaus Universitetas, fiziniai mokslai, fizika – 02P).

Nariai:

Prof. dr. (HP) **Gintaras Valiulis** (Vilniaus Universitetas, fiziniai mokslai, fizika – 02P).

Prof. habil. dr. **Valerijus Smilgevičius** (Vilniaus Universitetas, fiziniai mokslai, fizika – 02P).

Doc. dr. **Valdas Girdauskas** (Vytauto Didžiojo Universitetas, fiziniai mokslai, fizika – 02P).

Prof. habil. dr. **Gintautas Jurgis Babonas** (Puslaidininkų fizikos institutas, fiziniai mokslai, fizika – 02P).

Oponentai:

Prof. habil. dr. **Arūnas Krotkus** (Puslaidininkų fizikos institutas, fiziniai mokslai, fizika – 02P).

Dr. **Rimantas Grigonis** (Vilniaus Universitetas, fiziniai mokslai, fizika – 02P).

Disertacija bus ginama viešame Fizikos mokslo krypties tarybos posėdyje 2009 m. liepos mėn. 2 d. 15 val. Vilniaus universiteto Fizikos fakulteto 510-oje auditorijoje. Adresas: Saulėtekio al. 9, 3 korp. LT-10222, Vilnius, Lietuva.

Disertacijos santrauka išsiuntinėta 2009 m. birželio mėn. 2 d.

Disertaciją galima peržiūrėti Vilniaus universiteto, Fizikos instituto bei Lietuvos nacionalinėje Martyno Mažvydo bibliotekoje.

## *Acknowledgment*

I would like to thank my supervisor Prof. A. Dubietis for ideas, remarks, excellent leadership and patience.

I would like to express my gratitude to Prof. A. Stabinis for consultations and particularly deep study and corrections of this work.

I am thankful to all coworkers and coauthors: A. Matijošius, G. Tamošauskas, A. Varanavičius, S. Minardi, A. Gopal, D. Faccio, F. Bragheri, A. Averchi for excellent scientific atmosphere in the laboratories and P. Di Trapani, A. Couairon ir E. Gaižauskus, M. Porras for ideas and theoretical knowledge.

I would like to thank the Department of Quantum Electronics at Vilnius University for highest level laser physics school in Lithuania.

I am particularly thankful to my family and friends for strong moral support.

## Table of Contents

1	INTRODUCTION.....	7
	1.1 Objectives .....	9
	1.2 Propositions to defend .....	9
	1.3 Novelty.....	10
	1.4 Approbation .....	11
2	PROBLEMATICS OVERVIEW .....	13
3	SPATIO-TEMPORAL CHARACTERIZATION OF LIGHT WAVE PACKETS	15
4	DYNAMICS OF THE ANGULAR SPECTRA .....	24
5	MEASUREMENT OF REFRACTIVE INDEX CHANGE AND FREE- ELECTRON PLASMA DENSITY .....	31
6	CONCLUSIONS.....	38
7	REFERENCES.....	39

# 1 Introduction

The phenomena associated with self-focusing of laser beams have been investigated since laser invention [1]. This kind of nonlinear propagation of a wave in a transparent medium particularly depends on the transversal intensity profile and power of the laser beam. Self-focusing is self-induced (Kerr) lens effect. In the case of long pulses or continuous wave laser radiation, self-focusing phenomenon is responsible for the damage of optical elements [2] and appears to be the main limiting factor in the development and production of high power laser systems. A number of physical processes in the medium are being initiated by self-focusing, therefore it is readily applied in the laser technology for modification of various properties of transparent materials. Kerr lens effect is widely used as mode-locking mechanism in laser cavity for generation of the shortest, few cycle optical pulses [3]. The phenomenon of phase modulation of a light pulse is strongly coupled with self-focusing of the laser beam and is widely used for development of coherent white light sources [4].

Recently, investigation of femtosecond ( $10 - 100$  fs) pulse interaction with matter has gained a considerable attention. Invention of femtosecond light sources provided an ability to affect the matter under intense laser irradiation without the optical damage, hence, the observation of light self-action processes without the optical break-down became possible, which was hardly achievable by the use of long (tens of ps or ns) laser pulses. Particularly, intense studies of formation and dynamics of light filaments in materials of different phase state are of great interest. While the laser beam is transforming into a light filament, it can propagate through clouds, thick mist or other highly turbulent and scattering media with minimal energy loss [5]. Such light filament in the height of tens of kilometers is able to initiate white light continuum generation, which can be used for spectroscopic analysis of the atmosphere gases, aerosols and pollutants [6]. By the use of light filamentation in gases, liquids and solid state materials, high power femtosecond white light continuum is generated, which is used for ultrafast spectroscopy applications and design of widely tunable parametric frequency converters [7]. Recent experiments show that by means of light filaments, parametric light amplification and generation of femtosecond pulses with Raman shift can be performed

in isotropic medium [8]. Light filaments propagating in noble gases generate intense pulses as short as few optical cycles ( $<5$  fs duration), which have a potential for generation of high order harmonics seeking for attosecond pulses in VUV and X-ray spectral range [9]. Intensive research of plasma channels created by femtosecond light filaments in air is being made. Electrical discharge can be initiated and set to any desirable direction by the use of these plasma channels [10]. Free electron density initiated by intense light filament is high enough to reflect microwaves. A cylinder formed by multiple light filaments is able to provide long range guiding of microwave beams without spreading [11]. Recent experiments also show that extraordinary properties of light filament induced plasma channel enable the generation of terahertz electromagnetic waves in the direction of laser beam [12]. The ionization of optically transparent solid state materials allows initiation of permanent structural changes in the medium and form narrow channels with altered refraction index (waveguides) in the bulk media [13]. This phenomenon can be utilized for synthesis of various microoptical elements, e.g. phase diffraction lenses [14], bulk wave splitters for telecommunication [15] and various photonic crystals or even photonic crystal lasers [16].

The initial shape of light wave packets changes dramatically in space and time during the self-action. The conventional pulse characterization methods, which refer to the measurement of space-integrated autocorrelation and crosscorrelation functions, allow us to obtain only partial information about the properties of emerging light pulse and their physical origins. Therefore, new measurement techniques are necessary to perceive and control the physical phenomena relevant to light-matter interaction and filamentation processes. Such measurements should allow the characterization of intensity distribution of the wave packet in the three-dimensional space at any moment in time and enable registration of instant structural changes of the medium. On the other hand, light-matter interaction processes are very fast and localized, thus their investigation demand both very high spatial (order of  $\mu m$ ) and temporal (order of fs) resolution.

The results of long-lasting research of nonlinear crystals and parametric phenomena provided the basis for the development of the ultrafast optical parametrical amplifiers [17]. These devices are able to generate few-cycle light pulses of very broad spectrum and tunable in wide frequency range. Optical parametrical amplifiers open the



door for new measurement techniques, which enable investigation of ultrafast light-matter interaction phenomena.

In this work, new measurement techniques are introduced and applied experimentally, which allowed high resolution temporal, spatial and spectral mapping of light wave-packet dynamics during the nonlinear propagation in transparent media, and enabled to observe and make accurate quantitative evaluation of the ultrafast change of medium properties.

### ***1.1 Objectives***

Investigation of spatio-temporal and spectral transformations of Gaussian wave packets in bulk nonlinear Kerr media with positive and negative group velocity dispersion, with high spatial, temporal and spectral resolution.

Investigation of the dynamics of instant refraction index change and plasma channel formation induced by nonlinear propagation of Gaussian wave packets in condensed media.

### ***1.2 Propositions to defend***

Femtosecond wave packet with initial Gaussian shape undergoing the self-action in the nonlinear Kerr medium transforms into a complex X-type conical wave. This transformation is governed by spatio-temporal dynamics of the wave packet, which causes redistribution of the energy. The character of the observed transformations is universal: in normal group velocity dispersion regime X-type wave is formed, which has characteristic X-shaped far-field angular spectrum distribution.

The form of the far-field angular spectral distribution of a wave packet is determined by the group velocity dispersion of the medium, which presets the phase conditions for the four-wave mixing and yields colored conical emission. In the anomalous group velocity dispersion regime, angular spectra of the radiation appear to be qualitatively different from the spectra obtained in the normal group velocity dispersion regime.

Initial Gaussian wave packet undergoing self-action in transparent nonlinear Kerr medium transforms into intense light filament, which initiates temporal variation of the refractive index and formation of a narrow plasma channel. The positive refractive index change is related to the nonlinear Kerr effect, while the negative refraction index change is related to free electron plasma.

### ***1.3 Novelty***

Design and development of three-dimensional laser mapping technique, which allowed precise recording of the spatio-temporal characteristics of light wave packets and their dynamics in transparent nonlinear Kerr media. By means of this technique we have demonstrated that in nonlinear Kerr medium the initial Gaussian wave packet undergoes irreversible modifications in space and time simultaneously, transforming into a conical X-shaped wave packet.

By applying the imaging spectrometer technique, which allows recording the far-field angular spectral distribution of a wave packet, it was identified that the group velocity dispersion of the medium and four-wave mixing determine the shape of observed angular spectra, which are typical for weakly localized X-waves.

Temporal and spatial parameters of light filament induced instantaneous refractive index change and plasma channel formation dynamics have been measured with high temporal and spatial resolution. This data is valuable from practical and fundamental viewpoint.

## **1.4 Approbation**

Material presented in the thesis is based on 6 papers published in the international scientific journals. Out of them, 5 papers are published in ISI-rated journals. The results were also presented at 11 international scientific conferences.

### **Author's publications**

1. A. Matijošius, J. Trull, P. Di Trapani, A. Dubietis, R. Piskarskas, A. Varanavičius, A. Piskarskas, Non-linear space-time dynamics of ultrashort wave-packets in water, *Opt. Lett.* **29**, 1123 (2004).
2. A. Matijošius, R. Piskarskas, E. Gaižauskas, A. Dubietis, P. Di Trapani, Space-time recovery of arbitrarily shaped wave-packets by means of three dimensional imaging technique, *Nonlinear Analysis: Modelling and Control* **9**, 259–270 (2004).
3. D. Faccio, A. Matijošius, A. Dubietis, R. Piskarskas, A. Varanavičius, E. Gaižauskas, A. Piskarskas, A. Couairon, P. Di Trapani, Near- and far-field evolution of laser pulse filaments in Kerr media, *Phys. Rev. E* **72**, 037601 (2005).
4. D. Faccio, A. Averchi, A. Couairon, A. Dubietis, R. Piskarskas, A. Matijosius, F. Bragheri, M. A. Porras, A. Piskarskas, P. Di Trapani, Competition between phase-matching and stationarity in Kerr-driven optical pulse filamentation, *Phys. Rev. E* **74**, 047603 (2006).
5. M. A. Porras, A. Dubietis, A. Matijosius, R. Piskarskas, F. Bragheri, A. Averchi, P. Di Trapani, Characterization of conical emission of light filaments in media with anomalous dispersion, *J. Opt. Soc. Am. B* **24**, 581 (2007).
6. S. Minardi, A. Gopal, M. Tatarakis, A. Couairon, G. Tamošauskas, R. Piskarskas, A. Dubietis, P. Di Trapani, Time-resolved refractive index and absorption mapping of light-plasma filaments in water, *Opt. Lett.* **33**, 86 (2008).

### **Conference presentations**

1. Matijošius, R. Piskarskas, A. Dubietis, J. Trull, A. Varanavičius, A. Piskarskas, P. Di Trapani, Space-time dynamics of ultrashort light pulses in water, Conference on Lasers and Electro-Optics, San Francisco, California, USA, CTuP33 (2004).
2. Matijošius, R. Piskarskas, A. Dubietis, J. Trull, A. Varanavičius, A. Piskarskas, P. Di Trapani, Space-time dynamics of ultrashort light pulses in water, Conference on Nonlinear Guided Waves and Their Applications, Toronto, Canada, TuD2 (2004).
3. Matijošius, R. Piskarskas, A. Dubietis, J. Trull, A. Varanavičius, P. Di Trapani, Space-time dynamics of ultrashort light pulses in water, International Workshop on parametric processes and periodical structures, Vilnius, Lithuania, 88 (2004).
4. R. Piskarskas, A. Matijošius, A. Dubietis, J. Trull, A. Varanavičius, P. Di Trapani, Three-dimensional mapping of complex wave-packets, XVI Lietuvos ir Baltarusijos seminaras „Lazeriai ir optinis netiesiškumas“, Vilnius, Lietuva (2004).

5. Matijošius, R. Piskarskas, A. Dubietis, J. Trull, A. Varanavičius, A. Piskarskas, P. Di Trapani, The investigation of temporal-spatial transformations of wave packets employing the laser tomography method, International Conference of Physics Students, Novi Sad, Serbia and Montenegro (2004).
6. O. Jedrkiewicz, J. Trull, D. Salerno, A. Matijošius, D. Faccio, A. Parola, P. Di Trapani, A. Dubietis, A. Varanavičius, G. Valiulis, E. Gaižauskas, R. Piskarskas, E. Kučinskas, G. Tamošauskas, M. A. Porras, F. Bragheri, V. Degiorgio, Nonlinear conical waves, International Workshop on optical parametric processes and periodical structures, Vilnius, Lithuania, 64 (2004).
7. R. Piskarskas, A. Matijošius, A. Dubietis, J. Trull, A. Varanavičius, P. Di Trapani, Savaiminis netiesinių X-impulsų formavimasis vandenyje, 36-oji Lietuvos nacionalinė fizikos konferencija, Vilnius, Lietuva, 236 (2005).
8. P. Di Trapani, Jedrkiewicz, D. Salerno, A. Matijošius, D. Faccio, A. Parola, A. Dubietis, A. Varanavičius, G. Valiulis, E. Gaižauskas, R. Piskarskas, E. Kučinskas, G. Tamošauskas, A. Piskarskas, M. A. Porras, F. Bragheri, V. Degiorgio, A. Couairon, Nonlinear conical waves for modern optical technology, International conference on coherent and nonlinear optics, St. Petersburg, Russia, IF11 (2005).
9. Matijošius, D. Faccio, P. Di Trapani, A. Dubietis, R. Piskarskas, A. Varanavičius, A. Piskarskas, E. Gaižauskas, A. Couairon, Spontaneous X-pulse generation in Kerr medium, European Conference on Lasers and Electrooptics, Munich, Germany, EC-1-2-TUE (2005).
10. R. Piskarskas, A. Dubietis, D. Faccio, A. Averchi, Waveguide inscription in BK7 glass by pre-formed X-pulses, ICONO/LAT Conference, Minsk, Belarus, ICONOLAT-47 (2007).
11. R. Piskarskas, A. Dubietis, D. Faccio, A. Averchi, T. Balčiūnas, A. Melninkaitis, P. Di Trapani, Waveguide inscription in transparent material by pre-formed X-pulses, 37-oji Lietuvos nacionalinė fizikos konferencija, Vilnius, Lietuva, S4-19 (2007).

## 2 Problematics overview

Shortly after laser invention, the research on nonlinear light-matter interaction have become relevant. It was perceived that for high intensity light pulses propagating in a transparent medium self-focusing of laser beam occurs, which causes optical breakdown of the matter. Already in 1964, with participation of one of the laser inventors C. H. Townes, self-focusing phenomenon and light filament formation has been predicted theoretically [1]. In the case of strong light-matter interaction the refraction index of the medium becomes dependent on the intensity of the propagating wave, consequently the light beam is able to transform into very narrow light filament, which further propagates without changing its spatial dimensions. In the wake of invention of powerful nanosecond lasers in 1966, the formation of light filaments was demonstrated experimentally in CS<sub>2</sub> liquid by the use of Q-switched ruby laser [18].

For initial Gaussian laser beam transforming into a filament in transparent medium, many physical effects come into play. Yet, the two main nonlinear physical mechanisms can be pointed out. On one hand, the optical Kerr effect, which forces the beam to self-focus. On the other hand, the multiphoton absorption limits the intensity of radiation and causes partial ionization of the medium, which locally decreases the refractive index and causes defocusing of the beam. Other physical mechanisms also play important role in the filamentation process: beam diffraction, pulse phase modulation, group velocity dispersion, self-steepening of the pulse, axial pulse splitting, beam refocusing cycles, etc.

The extensive experimental data base gave rise to numerous physical interpretations of the origin of light filaments.

**Moving focus model.** According to this model, the filament is formed by temporal segments of the light pulse, which have different power and therefore focus at different distances along the propagation axis [19]. This interpretation is suitable only for longer pulses and it does not explain many other important processes observed during femtosecond filamentation.

**Spatial soliton model.** This model interprets the filament as a spatial soliton which is formed in the dynamic equilibrium among self-focusing, diffraction and plasma

defocusing [20]. This model, however does not properly explain the origin of spontaneous formation of the conical wave and self-reconstruction of its central peak [21].

**Dynamic spatial replenishment model.** This model interprets the light filament as a sequence of refocusing cycles [22]. This interpretation does not explain conical emission.

**Conical wave model.** This model interprets the light filament as a conical wave propagating in a medium [21] and explains the self-reconstruction of central peak. Multiphoton absorption plays an important role in formation of the conical wave as the central part of Gaussian beam is being absorbed stronger than the peripheral radiation. This model well explains the most of spatial beam transformations. However it does not count for pulse duration.

**X-wave model.** On the background of conical wave model a new more fundamental X-wave model has been proposed. This interpretation refers to spontaneous formation of the nonlinear X-waves [23] and takes in account short pulse duration, spectral broadening and free electron plasma. Nonlinear X-waves generalize linear X-wave concept in the nonlinear medium. Linear X-waves are weakly localized stationary wave packets in dispersive medium, which consist of coherently combined monochromatic Bessel beams of different frequency that propagate with different cone angles preserving a particular dispersion law. The X-wave model treats conical emission as undetachable part of the wave packet. The nature of conical emission is phase-matched four-wave mixing.

In the wide field of light filamentation interpretations, the correct answer about the importance of above-mentioned physical processes can be given only by experiments, which allow for high resolution measurement of the wave packet and medium alterations in time and space simultaneously. Therefore, in this work, the focal attention is given to the development and experimental implementation of such measurement techniques.

### 3 Spatio-temporal characterization of light wave packets

#### Diagnostic techniques for arbitrary shaped wave packets

The major problem related to experimental characterization of the wave packet dynamics is that most of the measurements have been limited either to pure temporal domain, by standard on-axis auto or cross correlation technique, or to the pure spatial one, by time-integrated CCD-based detection. Although these techniques provide useful information on pulse or beam characteristics, and could be extended by incorporation of frequency resolved optical gating (FROG), they are not capable to ensure complete space-time characterization of the resulting wave-packet. To date, few efforts in providing complete space-time characterization of ultrashort wave-packets had not been successful. An example has been reported in [24]. The used technique, based on optical polarigraphy, has shown indeed a quite poor resolution, and did not allowed the fine details of the spatio-temporal structure to be recovered. It should be noted that to date most of space-time characterization techniques require complex numerical data processing algorithms.

In recent works related to the investigation of the nonlinear dynamics of X-waves in quadratic non-linear media a very powerful, high spatio-temporal resolution 3D-mapping technique has been proposed, based on the use of ultrafast  $\chi^2$  gate [25]. The approach resembles the crosscorrelation measurement to some extent, but instead of recording the space-integrated (or simply on-axis) signal, the entire space-time resolved sum-frequency intensity profile is captured.

In this work we have applied and improved laser 3D-mapping technique for the investigation of transformations of the ultrashort pulses in transparent isotropic media. We were able to increase spatial and temporal resolution up to 10 times. This technique enables us to observe the results in real time without the need of complex numerical processing algorithms.

#### Three dimensional imaging technique

The principle of three dimensional imaging technique could be described as follows. Fig.1 illustrates the basic idea of the method: for a chosen time delay, short

probe pulse interacts with a short temporal slice of the test wave-packet within the nonlinear crystal, and generates the sum-frequency signal.

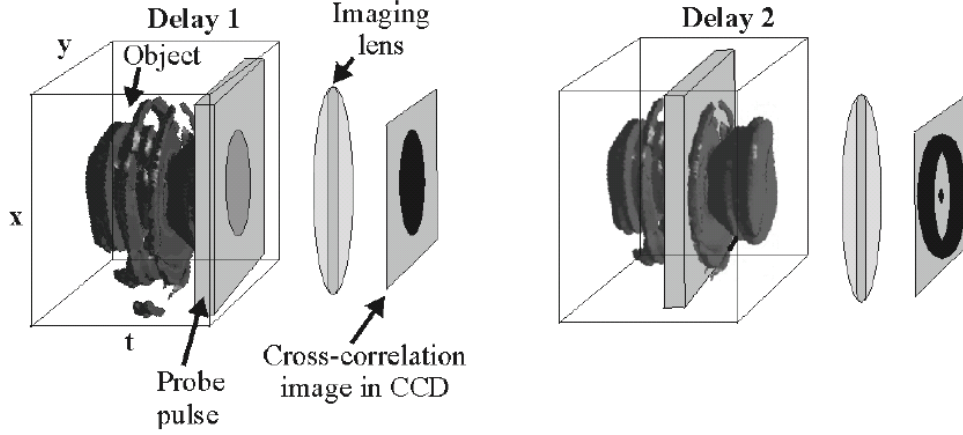


**Fig. 1.** Schematic representation of three dimensional imaging technique.

Its fluence profile is then imaged and recorded by a CCD camera. Then by spanning the delay time, the assembly of time slices is collected. The spatio-temporal intensity map of the test wave-packet is then reconstructed with high temporal and spatial resolution being defined by the duration of the probe pulse.

Let's consider the wave packets of an object ( $E_O$ ) and a probe pulse ( $E_P$ ):

$$\bar{E}_O = E_O(x, y, z, t)e^{i[\omega_O t - k_z(\omega_O)z - k_x(\omega_O)x]} + c.c., \quad (1)$$

$$\bar{E}_P = E_P(x, y, z, t)e^{i[\omega_P t - k_z(\omega_P)z - k_x(\omega_P)x]} + c.c. \quad (2)$$

Here complex functions  $E_O(x, y, z, t)$  and  $E_P(x, y, z, t)$  are slowly varying wave amplitude profiles of frequencies  $\omega_O$  or  $\omega_P$ . These two equations describe propagation along  $z$  axis of two waves which intersect in the  $(x, z)$  plane with an angle  $\theta = 2 \arctan(k_x/k_z)$ , where  $k = \sqrt{k_x^2 + k_z^2} = 2\pi/\lambda$ . The polarization determining the sum-frequency generation in quadratic medium may be written in the following way:

$$P_{SF} \propto 2E_O E_P e^{i[\omega_{SF} t - k_z(\omega_{SF})z]} + c.c. \quad (3)$$



Here one must consider the phase matching and energy conservation conditions:

$$k_z(\omega_{SF}) = k_z(\omega_O) + k_z(\omega_P), k_x(\omega_O) = -k_x(\omega_P) \text{ and } \omega_{SF} = \omega_O + \omega_P. \quad (4)$$

Suppose that the sum frequency field propagates in  $z$  direction and has slowly varying amplitude function  $E_{SF}(x,y,t,z)$ . The spatio-temporal intensity profile of the object's wave packet will be undistorted if we make 3 assumptions:

1. Low energy conversion for fields  $E_O$  and  $E_P$ ;
2. Low diffraction and dispersion in the crystal;
3. Group velocity mismatch of interacting waves can be neglected:  $U_O=U_P=U_{SF}=U$ .

The assumptions will be qualified only in the case when the nonlinear crystal is as thin as possible and the beams are of large diameter. These assumptions allow to find a traveling reference frame for all the propagating pulses by introducing the retarded time  $\tau = t - z/U$ . A set of partial differential equations describing the interaction process then reduces to an ordinary differential equation for the envelope  $E_{SF}$ . If we also introduce a time delay  $\tau_i$  on the reference wavefront, the equation takes the form:

$$\frac{dE_{SF}(x, y, \tau, z)}{dz} = i2\sigma E_O(x, y, \tau, z)E_P(x, y, \tau - \tau_i, z), \quad (5)$$

where  $\sigma$  is the non-linear coupling coefficient. The last equation is readily integrated and, if the mixing crystal is placed at position  $z_0$ , its solution reads:

$$E_{SF}(x, y, \tau, z_0) = i\sigma 2E_O(x, y, \tau, z_0)E_P(x, y, \tau - \tau_i, z_0)\Delta z. \quad (6)$$

This equation shows that the spatio-temporal profile of the sum frequency wave packet is proportional to the spatio-temporal profile of the object's wave packet. By imposing a set of delays ( $\tau_i, i=1, \dots, n$ ) to the reference wave packet with respect to the object, a reliable 3D reconstruction of the wave packet structure can be achieved by the collection of the  $n$  images  $S(x,y,\tau_i,z_0)$ . By changing the plane  $z_0$ , the temporal evolution of the wave packet can also be obtained.

The temporal resolution of this technique is determined by the duration of the probe pulse. The spatial resolution is determined by aperture size of CCD matrix, magnifying telescope and sum-frequency crystal.

### **Experimental setup**

The experimental layout consists of four different blocks: (a) the test (arbitrarily shaped) wave-packet generator; (b) the probe pulse generator; (c) nonlinear gate; (d) data acquisition system.

(a) The test (arbitrarily shaped) wave-packet was excited by launching spatially filtered and focused 0.9  $\mu\text{J}$ , 150 fs, 527 nm pulses into a syringe shaped water cell using  $f = 500$  mm lens. The input pulses were generated by a frequency up-converted optical parametric amplifier (TOPAS, Light Conversion Ltd.), pumped by 100 fs, 800 nm pulses delivered by a Ti:Sapphire laser system (Spitfire, Spectra Physics) at 1 kHz repetition rate. With the input power 5 times above critical power for continuous wave self-focusing ( $P_{crit} = 1.15\text{MW}$  in water at  $\lambda = 527$  nm as derived from a standard equation  $P_{crit} = 3.77\lambda^2/8\pi n_0 n_2$ ,  $n_2 = 2.7 \times 10^{-16}$   $\text{cm}^2/\text{W}$ ), a single filament with white light spectrum content and FWHM diameter of 45  $\mu\text{m}$  was excited.

(b) High intensity contrast, 20 fs and 13  $\mu\text{J}$  probe pulse with wavelength centered at 710 nm was provided by a non-collinear optical parametric amplifier (TOPAS White, Light Conversion Ltd.) pumped by a frequency doubled Ti:Sapphire laser pulses and has 1 mm FWHM diameter.

(c) Sum frequency mixing process between the test and the probe pulses in a thin (20  $\mu\text{m}$ ) type I phase-matching  $\beta$ -barium borate (BBO) crystal served as a nonlinear gate. In order to avoid severe distortions of the test pulse spatial profile imposed by free-space propagation, it has been imaged onto the input face of the nonlinear crystal by means of a magnifying telescope. Sum-frequency signal centered at 302 nm was then imaged onto the high dynamic range CCD camera. In this configuration, the field obtained via sum-frequency generation in BBO crystal resulted in a fluence distribution  $(x, y, t_1, z_0)$  at given delay  $t_1$ . In order to obtain sum-frequency signal proportional to the object intensity, where  $z_0$  corresponds to the fixed plane selected by the imaging telescope ( $z_0=0$  at the water cell output-face plane), we employed a probe pulse with constant intensity over the

area of the test wave-packet to be characterized (note 1 mm FWHM diameter), and ensured that sum-frequency generation process is performed in the low conversion limit. Then by spanning the delay  $t$  by a motorized stepper motor (12 fs steps), the complete intensity map  $I(x,y,t,z_0)$  can be retrieved, the ultimate temporal resolution being defined by the probe pulse width, by its front steepness and by its intensity contrast. We note that temporal, as well as spatial walk-off between the test and probe wave packets were negligible for such a thin crystal. The sequence of sum-frequency fluence profiles that correspond to different delay times is sketched in Fig.2.

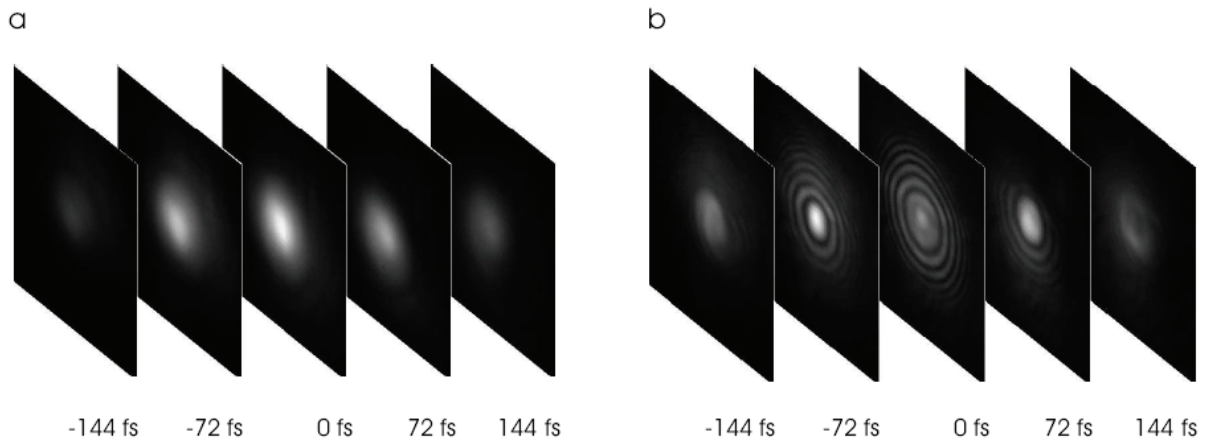
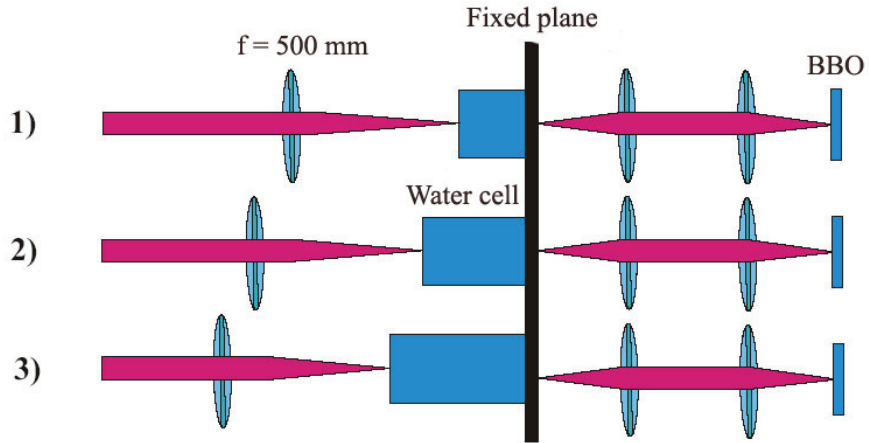


Fig. 2. Time resolved intensity profiles of the wave packet: (a) input Gaussian wave packet  $I(x, y, t, z = 0 \text{ mm})$ ; (b) test wave packet after self-focusing  $I(x, y, t, z = 22 \text{ mm})$ . Negative and positive delay times denote the leading and the trailing edges of the pulse, respectively.

(d) The image acquisition was performed by imaging the output face of the BBO crystal onto a CCD detector (Andor Technology) and by acquiring the fluence profile of the sum-frequency signal for different time delays. The use of a high dynamic (16 bit/pixel), low noise (cooled down to  $-50^{\circ}\text{C}$ ) CCD with background subtraction allowed us to perform high sensitivity and high dynamic range detection, while keeping very low energy conversion in the sum-frequency process. Typically, CCD on-chip integration of over 1000 shots has been performed.

### Experimental results

By changing the length of the water cell (as schematically depicted in Fig.3) images for different propagation distances  $z$  of the wave packet can be recorded.



**Fig.3.** The principle of length variation of the water cell while keeping imaging plane fixed.

The main set of the results yielding complete characterization of the test wave packet is depicted in Figs.4-5.

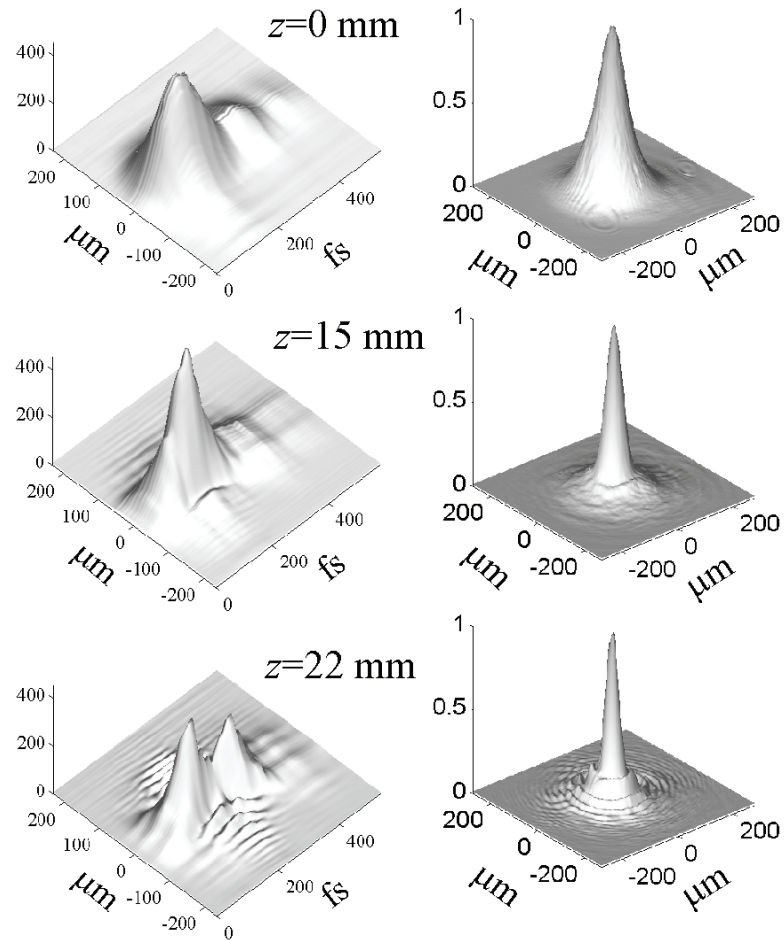


**Fig.4.** Evolution of space-time intensity (left) and normalized time-integrated fluence (right) profiles versus  $z$  of 527 nm, 150 fs pulse propagating in water at  $P = 5P_{\text{crit}}$ .

By means of time-integrated spatial detection, we measured a single filament of  $\sim 45 \mu\text{m}$  FWHM diameter, which is formed at  $z = 15 \text{ mm}$ , being surrounded by oscillating annular ring structure (right panel of Fig.4). This structure persists over the investigated  $z$  range, with slight changes in the diameter of the central spike. Left panel of Fig.4 illustrates the spatio-temporal intensity profiles of the reconstructed wave packet at different  $z$ , as measured by changing length of the water cell. The space-time maps show evident pulse compression at  $z=15 \text{ mm}$ , on axis splitting at  $z = 22 \text{ mm}$ , followed by the recombination at  $z = 30 \text{ mm}$  (not shown here). Out of the beam axis intense modulated wings appear, whose intensity remain peaked at the pulse central temporal coordinate. This last feature is particular important if one accounts that the major part of the wave-packet energy is indeed contained into the outer part of the beam. In fact, direct measurements by means of pinholes and stoppers had shown that the central spike (filament) contains less than 20% of the total energy.

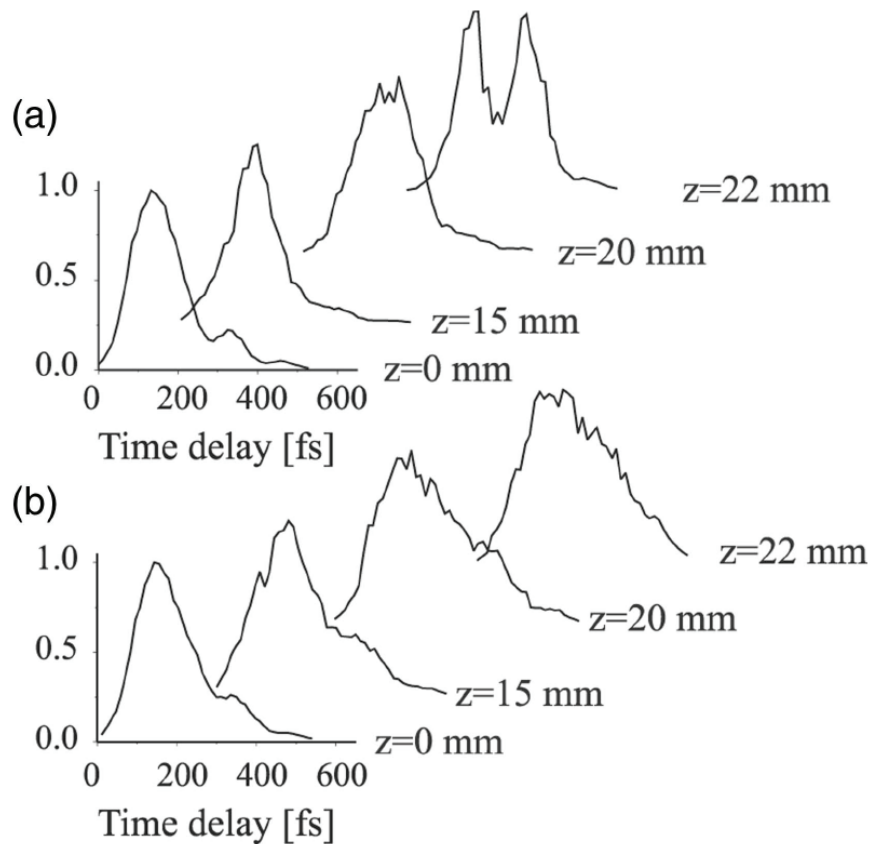


**Fig.5.** (a) Normalized intensity (temporal) profiles at the beam center,  $I(x=0, y=0, t, z)$ , and (b) normalized power profiles,  $P(t, z)$ , for different propagation lengths,  $z$ .

These results let us foresee that pulse recombination could appear because of refocusing of a portion of a power distributed in these intense outer rings. Deeper analysis shows that alleged pulse splitting does not refer to entire wave packet, but just to very central portion of it, as the power (space-integrated intensity) distribution remains peaked at the pulse center at any value of  $z$  (see Fig.5).

Similar measurements were performed for different wavelengths and energies of the initial pulse. The parametric generator (TOPAS) has been removed out of the setup and 800 nm, 133 fs pulses straight from laser (SPITFIRE) have been focused on the water cell. The most relevant and illustrative results are depicted in Fig.6 as spatio-temporal fluence maps for different initial pulse energies  $\varepsilon$  and different propagation distances  $z$  in water.

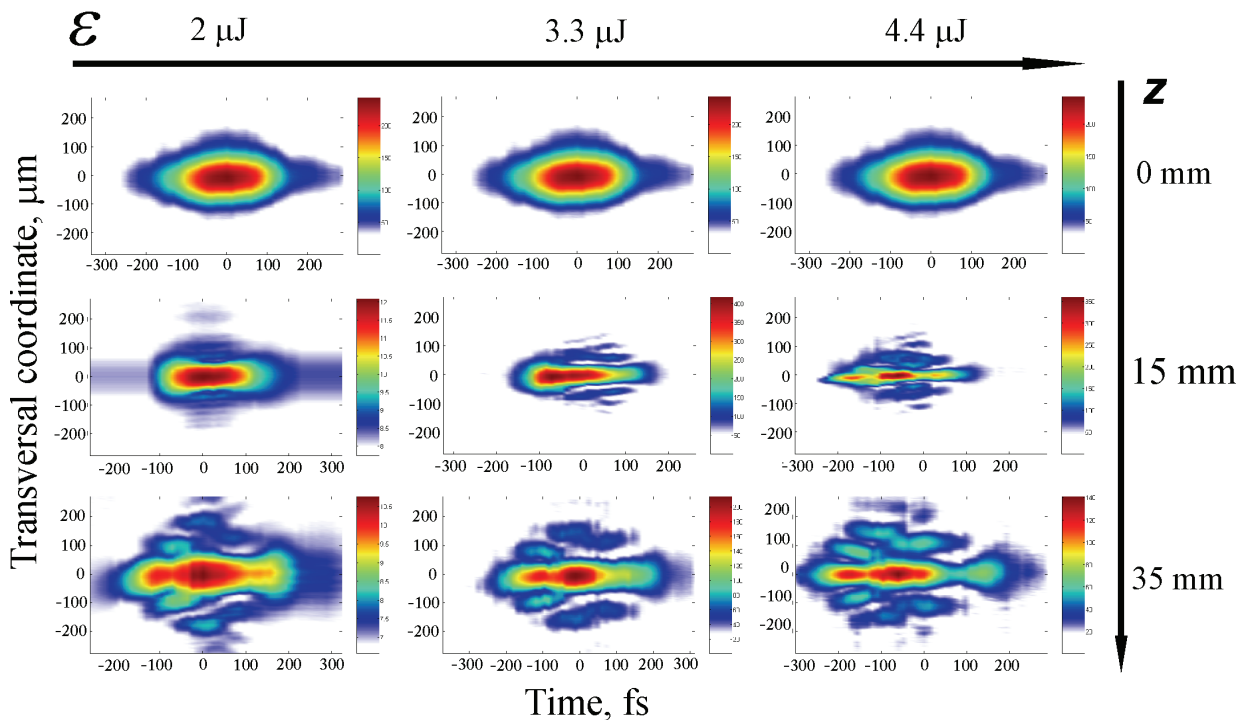


**Fig.6.** Transformation dynamics of 800 nm and 133 fs pulses for different initial pulse energies and different self-action lengths in water.

The comparison of the experimental results for two different initial pulse wavelengths and various energies let us make the following conclusions. The initial Gaussian pulse transforms into a conical wave with intense on-axis component, however, most of the energy is transferred to the beam periphery. Preliminary results point to

complex space-time dynamics, which is ruled mainly by the interplay between self-focusing, chromatic dispersion, nonlinear losses and diffraction. The observed pulse splitting and recombination characterize just on-axis temporal intensity profile, but not the wave packet as a whole. These effects seem to occur in conjunction with relevant energy exchange between the beam center and the self-built, slowly decaying, oscillating tails. This kind of energy redistribution causes the origin of X-type intensity profile of the wave packet. These properties are universal for wave packets undergoing self-focusing in normal group velocity dispersion region.

The 3-dimensional laser mapping technique allows very precise analysis of near-field spatio-temporal intensity distribution of ultrashort wave packets. Additionally, for deeper investigation and characterization of arbitrary shaped wave packets, measurements of temporal and spatial spectra must be performed.

## 4 Dynamics of the angular spectra

For complete characterization of the wave packet undergoing self-focusing, additionally to spatio-temporal mapping one requires to investigate the far-field angular spectrum which gives information about spacial distribution of wave packet's spectral components.

### Imaging spectrometer technique

Measurement of the far-field angular spectra  $(\theta, \lambda)$  is based on the angular spectrometer technique. The experimental setup is depicted in Fig.7.

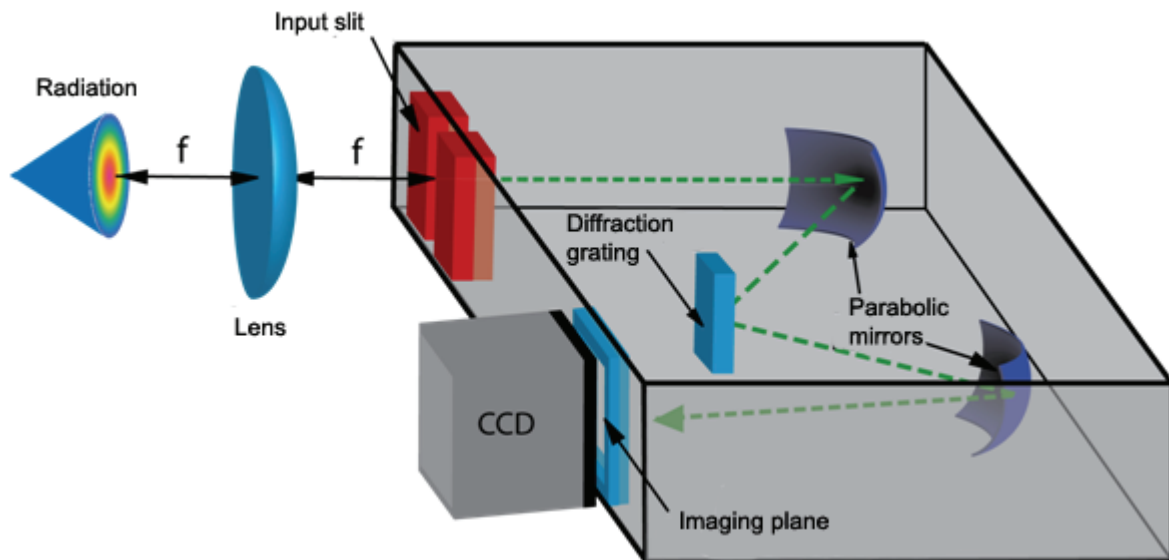


**Fig.7.** Experimental setup of imaging spectrometer technique for measurement of far-field  $(\theta, \lambda)$  spectra.

Assume we have a wave packet with complex spatio-temporal structure and broad spectrum. Let's put a lens with focus length  $f$  assuring that we collect all the radiation. At the distance  $f$  behind the lens, we will have the plane where spatial Fourier transform of the radiation will occur, i.e. the transverse intensity profile  $(x, y)$  of the wave packet will be transformed into its Fourier components at  $(\theta_x, \theta_y)$  coordinates. At this plane we put a narrow vertical slit. The imaging spectrometer, which consists of a diffraction grating



and two parabolic mirrors, will reproduce the vertical intensity profile (i.e.  $\theta_y$  profile) at its output (imaging) plane. However in the horizontal direction, the radiation will be frequency resolved. Hence, the horizontal axis at the output of spectrometer will show a spectral profile (i.e. wavelengths  $\lambda$ ) and the vertical axis will correspond to spatial Fourier transform (i.e. angles  $\theta$ ). At the imaging plane we put a high dynamic range CCD camera which is able to capture the whole 2D image. The wavelength scale can be calibrated by rotating the diffraction grating so that we shift the central wavelength by  $\Delta\lambda$  and count the number of CCD pixels  $N$  that the central wavelength has moved by. The calibration constant is calculated as  $C_\lambda = \Delta\lambda/N$  [nm/pixel]. Vertical axis is calibrated as  $C_\theta = \Delta Y/f$  [rad], where  $\Delta Y$  is the height of a CCD pixel.

In this work we applied imaging spectrometer technique for measuring of the angular spectra ( $\theta$ ,  $\lambda$ ) of ultrashort light wave packets experiencing transformations during the filamentation process. Several experiments on angular spectra measurement are presented. Two different media for light self-focusing are compared – water and fused silica. Additionally, the angular spectra for various dispersive conditions are compared – in normal and anomalous group velocity dispersion regime, and in the transition regime around the dispersion zero.

### **Normal dispersion regime**

In this experiment, filamentation was induced in the water sample by launching 160 fs pulses with wavelength centered at 800 nm. The pulses were loosely focused onto the water-cell input facet with a 500 mm focal-length lens (the beam diameter at the cell input was 80  $\mu\text{m}$  FWHM) and an input energy of  $\varepsilon = 3.3 \mu\text{J}$  ( $P = 11P_{crit}$ ). A set of measurements was performed, where we characterized the angular spectra ( $\theta$ ,  $\lambda$ ) for various propagation lengths  $z$  by collecting the whole filament with a lens, placed so as the Fourier plane falls on the entrance slit of an imaging spectrometer (MS260i, Lot-Oriel). The output ( $\theta$ ,  $\lambda$ ) spectrum is then recorded on a 16-bit CCD camera (DU420, Andor).

Fig.8 shows the dynamics from the input pulse (a) to a generally broadened spectrum at  $z=1$  cm (b), followed by the appearance of the colored conical emission, i.e., structures with a definite ( $\theta$ ,  $\lambda$ ) dependence, at  $z=2$  cm (c). Further propagation leads to

an intense axial continuum generation at  $z=3$  cm [Fig.8 (d)] along with the enhancement of the conical emission, with the appearance of X-like features, albeit with a marked asymmetry (the redshifted long X-tails seem to be missing). This angular dispersion results from the interplay between the Kerr nonlinearity, diffraction, and chromatic dispersion, or, analogously, from a strong space-time coupling.

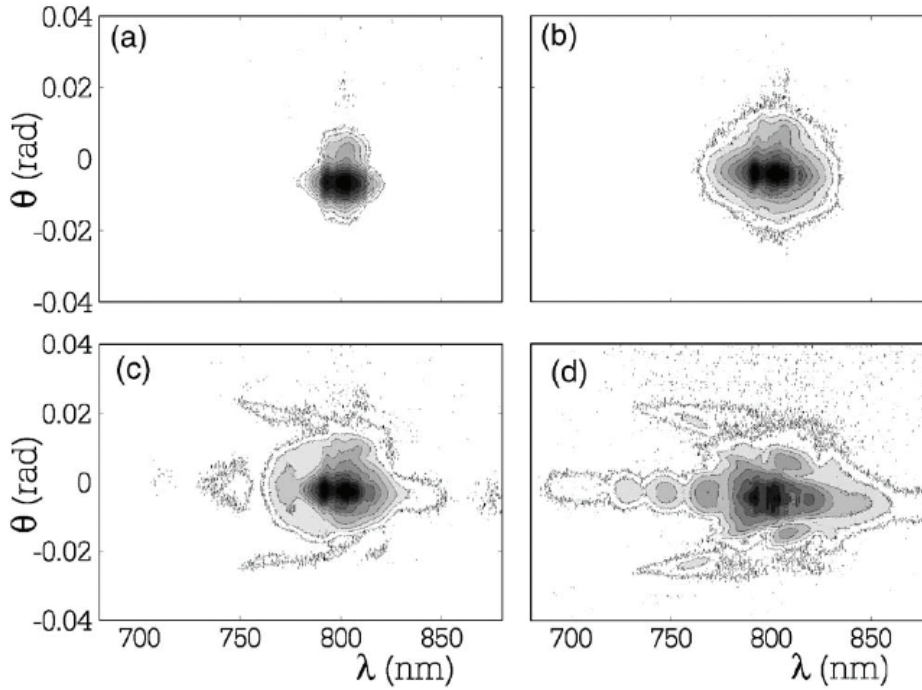


**Fig.8.** Experimental  $(\theta, \lambda)$  spectra for various lengths  $z$  of the water cell. (a) Input pulse, (b)  $z=1$  cm, (c)  $z=2$  cm, (d)  $z=3$  cm. The input pulses: 800 nm,  $\epsilon=3.3$   $\mu\text{J}$ .

The linking of spatio-temporal 3D mapping results with far-field angular spectra data shows that the far-field angular spectrum takes a form of X as the initial Gaussian wave packet undergoing self-focusing in Kerr media with normal group velocity dispersion transforms into X-type wave.

### **Transition between normal and anomalous dispersion**

The experiments were performed in two different nonlinear Kerr media, i.e., in pure water and fused silica. The input laser pulse was delivered from a Nd:glass laser (Twinkle; Light Conversion Ltd.) and a tunable optical parametric generator (TOPAS; Light Conversion Ltd.). The pulse had 200 fs duration (FWHM) and was loosely focused

down to 100  $\mu\text{m}$  diameter (FWHM) at the sample input facet. In order to induce filamentation the input energy  $\varepsilon$  was typically varied from 2 to 20  $\mu\text{J}$  so that the input power was  $P = 5\text{--}20 P_{crit}$ . Laser wavelength was chosen to be: 1055 nm for water, i.e., just slightly larger than the zero-dispersion wavelength ( $\sim 1000$  nm), and 1600 nm for fused silica, i.e., well within the anomalous dispersion regime. In the water experiment, owing to negligible second-order dispersion, we expect third-order or more generically high-order dispersion (HOD) to play a dominant role. In the fused-silica experiment, in contrast, the wavelength was chosen far from the zero-dispersion region (1290 nm). Even in this case, however, the nonlinear dynamics provided evidence of a relevant HOD effect. The filament generated inside the Kerr medium was collected from the output sample facet and imaged by a double-lens telescope onto the focal plane of an  $f = 15$  cm focal-length lens. This lens was in turn positioned at a distance  $f$  from the input slit of an imaging spectrometer (MS260i, Lot-Oriel). The  $(\theta, \lambda)$  far-field profile at the output of the spectrometer was recorded on a CCD camera. In Fig.9 we show a single-shot angular spectrum of a filament generated in 4 cm of water, for the case of  $\varepsilon = 15$   $\mu\text{J}$ . The angular spectrum is highly asymmetric, with ring-like interference fringes surrounding the pump, and a hyperbolic-like tail peaked at  $\sim 850$  nm and extending further in the blue-shifted region. The input-pump angular spectrum is shown in the inset to Fig.9 for a comparison.

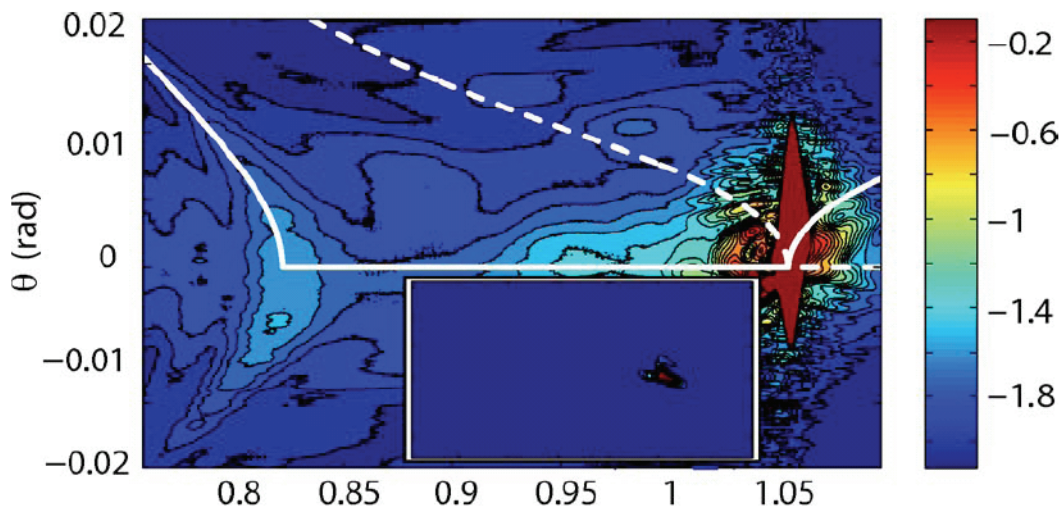


**Fig.9.** Experimentally measured log-scale spectrum of a filament in 4 cm of water, with an input pump centered at 1055 nm and with  $\varepsilon = 15$   $\mu\text{J}$ . The inset shows the input spectrum on the same scale, but with shifted axis. White solid lines indicate the stationary fish-like mode.

In Fig.10 we show a similar spectrum for the case of fused silica with  $\epsilon=5 \mu\text{J}$ . The spectrum here was frequency doubled before the spectrometer using a 20- $\mu\text{m}$ -thick BBO crystal, so as to shift the wavelengths into the silicon-based CCD sensitivity range. In order to capture the exceptionally large spectral bandwidth, Fig.10 is composed of spectral samples belonging to different shots, but all taken with very similar ( $\pm 3\%$ ) input energies. As in Fig.9 we note the marked asymmetry, with elliptical features around the input wavelength and a hyperbolic modulation at blue-shifted wavelengths.

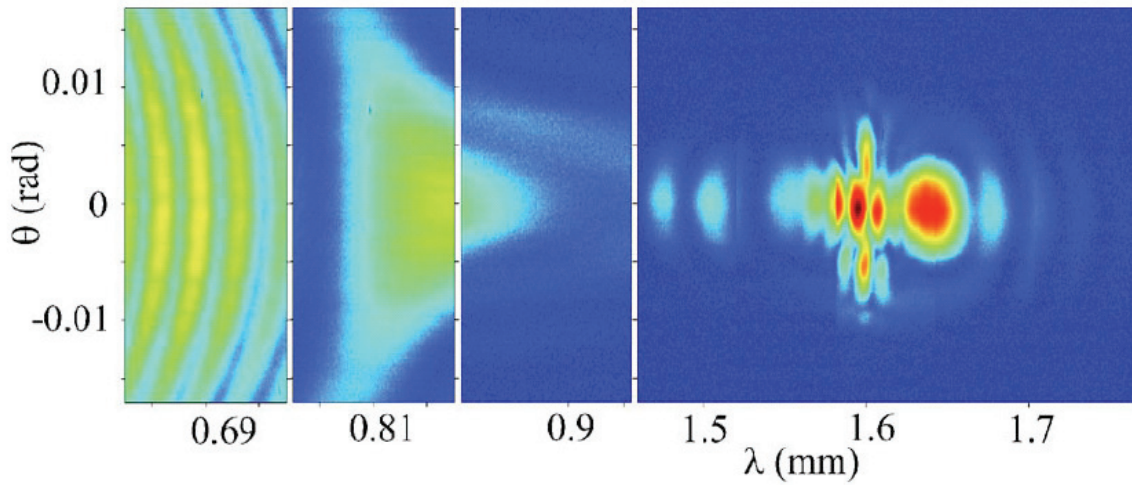


**Fig.10.** Experimentally measured spectrum of a filament in 3 cm of fused silica with an input pump centered at 1600 nm and with  $\epsilon=15 \mu\text{J}$ .

### **Anomalous dispersion regime**

In this experiment we used a broadly tunable optical parametric generator (TOPAS, Light Conversion Ltd.) pumped by the second-harmonic-compressed 200 fs pulses at 527 nm generated by a mode-locked and regeneratively amplified Nd:glass laser (TWINKLE, Light Conversion Ltd.). Idler pulses from the optical parametric generator, tunable from 1055 to 2600 nm, were isolated by means of a Glan–Taylor polarizer, spatially filtered to ensure a clean Gaussian-like spatial profile, and then focused onto the input face of 41 mm long fused silica sample by using a  $f=500$  mm lens. Loose focusing geometry resulted in 80  $\mu\text{m}$  diameter (FWHM) focal spot at the entrance of the sample, and the input energy of the pulse ( $\sim 2.5 \mu\text{J}$ ) was adjusted so as to excite a single filament. Since our conventional Silicon-based data acquisition system

(10-bit CoHU CCD camera with Spiricon frame grabber) is not sensitive to the infrared wavelengths of interest (above 1100 nm), the output radiation from the sample was frequency doubled by means of a thin (20  $\mu\text{m}$  long) type-I phase matching  $\beta$ -barium borate crystal placed just after the sample. Short crystal length guaranteed broadband frequency conversion along with wide angular acceptance in the linear second harmonic generation regime. The frequency-doubled radiation was then analyzed by means of an imaging spectrometer technique that enables single-shot recording of  $(\theta, \lambda)$  spectra: the light focused on the rear focal plane of an achromatic, large aperture Fourier lens of focal length  $f = 50$  mm, encounters the input slit of the spectrometer (EG&G, Princeton Applied Research, with a 600 lines/mm grating), and its output image plane is recorded by the CCD camera. We have performed measurements of  $(\theta, \lambda)$  spectra launching pulses at 1400, 1500, 1600, and 1700 nm carrier wavelengths.

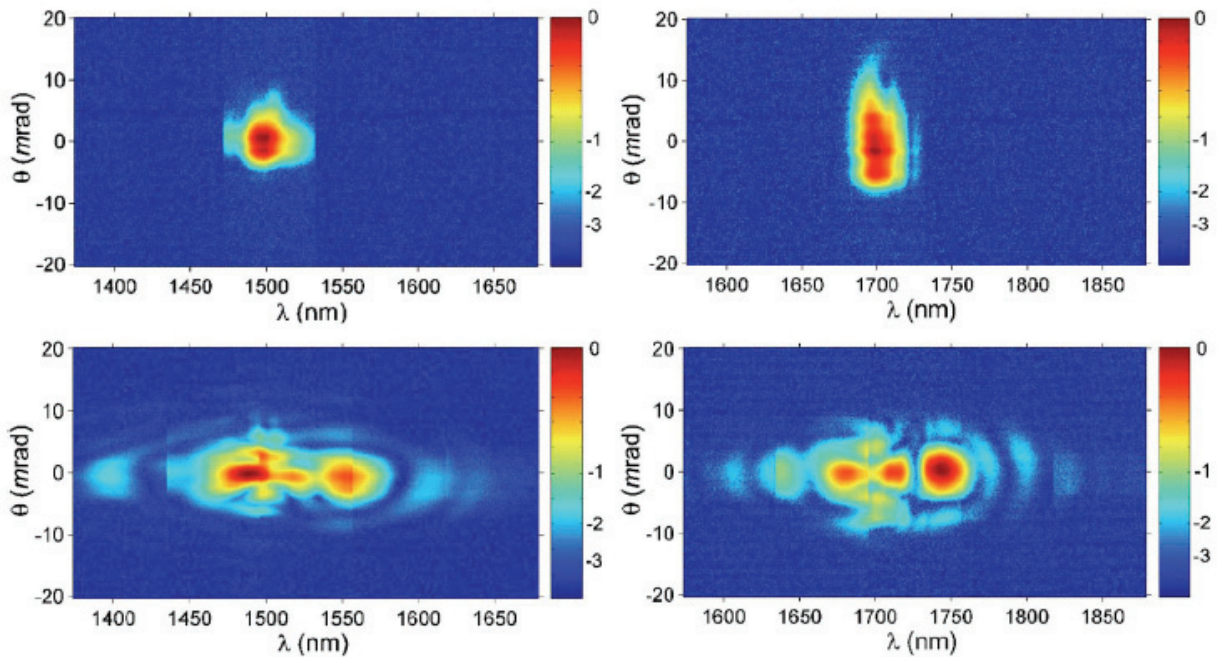


**Fig.11.** Angle-wavelength spectra (in logarithmic scale) of the input pulses at 1500 and 1700 nm carrier wavelengths (top) and of the corresponding output filaments from the fused silica sample (bottom).

Fig.11 compares the recorded spectra for input pulses at 1500 and 1700 nm when the fused silica sample is removed (top) and when it is inserted (bottom). As seen in Fig.11 (bottom), the onset of the axial spectral continuum characteristic of filamentation in the sample is accompanied by the appearance of nearly elliptical fringes. Similar

features are observed for the other carrier wavelengths. Owing to the high spectral resolution required to visualize the fringes, the overall 300 nm wide spectrum is composed of five spectra covering successive wavelength ranges and taken from different laser shots. The observed round, nearly elliptical structures sharply distinguish the angular dispersion recorded in material with anomalous group velocity dispersion from the X-like angular dispersion with material normal dispersion, and prove the generality of the phenomenon conical emission in anomalous dispersion featured by the decreasing emission angle with an increasing wavelength shift.

Experimentally, we showed that the shape of wave packet's far-field angular spectrum in the anomalous group velocity dispersion regime is quantitatively different from that observed in the normal group velocity dispersion regime. These results indicate that Kerr instability in the presence of diffraction and anomalous dispersion acts as a mechanism that pushes the pump pulse towards a configuration with spatiotemporal "spherical" symmetry.

## 5 Measurement of refractive index change and free-electron plasma density

Structural modifications or refractive index changes induced by focusing an ultrashort laser pulse in a transparent dielectric media are the basis of modern production of optical devices buried in bulk optical media, such as waveguides, gratings, and three-dimensional optical memories, as well as of biomedical applications such as refractive surgery. Around the focus, the laser pulse usually generates pairs of electrons and holes by optical field ionization. In case of a tight focusing configuration, the electron density is in turn all the more enhanced by inverse Bremsstrahlung, easily reaching  $10^{20} \text{ cm}^{-3}$  and inducing strong absorption. Ionization may initiate structural medium changes, which can be either temporal or permanent. There may be two types of mechanisms responsible for nondestructive structural change of transparent material initiated by strong radiation: color centers – related to electronic point defect in the medium lattice; and local density change – related to local stress of the lattice.

For collimated beams or small numerical apertures, the electron-hole plasma may be limited to lower densities, thereby allowing weak absorption and filamentary propagation of the laser beam. Postmortem of damaged materials provides an indirect estimation of the electron plasma density, but its direct measurement is a difficult task in the filamentation regime [26]. The small transverse size of the plasma channel ( $\sim 2\text{--}5 \mu\text{m}$ ) and the correspondingly small induced phase shift ( $\pm 0.01$  rad) make it difficult to perform interferometric or all-optical spatiotemporally resolved measurements. Previous measurements [27, 24] estimated plasma densities only for a tight focusing configuration in solids and liquids (including water) using electric conductivity measurements, polarography, interferometry, time-resolved holography, or absorptive shadowgraphy [28]. In all cases, the probe pulses were of the same duration as that of the pulse exciting the filament, therefore the dynamics of the formation of the plasma could not be resolved. From the fundamental viewpoint, a higher temporal resolution would be needed to assess the role of plasma in the propagation of the light filament, which might

be less significant in condensed media than in gases, as suggested by the recent reinterpretation of this phenomenon on the basis of the X-wave paradigm [29].

### Quantitative shadowgraphic method

According to geometrical optics, in a homogeneous medium optical rays belonging to a collimated uniform beam of intensity  $I_0$  propagate parallel to each other in the longitudinal direction  $z$ . The rays hitting a transparent, optically thin object are deflected by its transverse gradients of refractive index and result in a transverse intensity pattern  $I(x, y)$  (the shadowgram) at an observation plane placed at a distance  $L$  from the object (see Fig.12.).

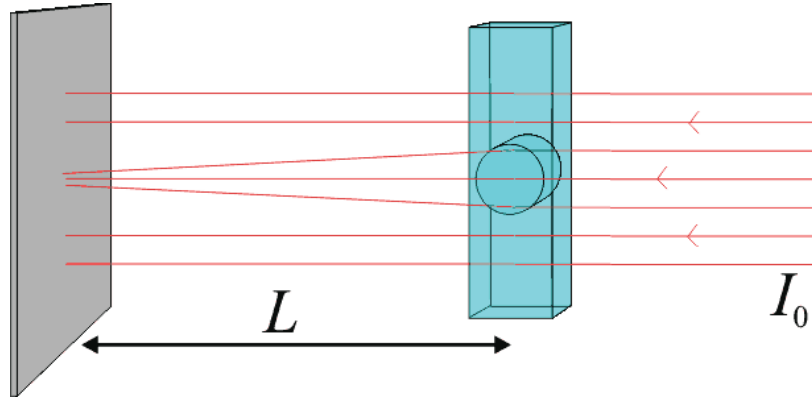


**Fig.12.** The principle of the shadowgraphic method. Parallel rays, which pass through a transparent object with refractive index variation, on screen, form an image of uneven intensity distribution.

By assuming negligible diffraction effects, small angle deflection, and the thickness of the sample  $\Delta z \ll L$ , it is possible to relate the transverse variation of the optical path of the sample to the shadowgram [30]:

$$\left( \frac{\partial^2}{\partial x^2} + \frac{\partial^2}{\partial y^2} \right) \int_0^{\Delta z} n(x, y, z) dz = -\frac{1}{L} \frac{I(x, y) - I_0}{I_0}, \quad (7)$$

where  $n(x, y, z)$  is the refractive index distribution of the phase object. It is easy to recognize in Eq. (7) the Poisson equation: the unknown is the optical path of the object, while the source term is proportional to the normalized intensity variation of the



shadowgram with respect to the intensity of the incoming plane wave. For radially symmetric samples, like light filament, the projection (shadowgram) will be related with the object's refractive index distribution via Abel transform [31]:

$$S(y) = 2 \int_y^R n(r)(r^2 - y^2)^{-1/2} r dr , \quad (8)$$

where  $S(y)$  correspond to distribution of the projection, and  $n(r)$  is refractive index distribution of the object. The Abel inversion transform can be applied to the optical path data to retrieve the three-dimensional refractive index distribution  $n(r)$  which in turn is proportional to the plasma density radial profile:

$$n(r) = -\frac{1}{\pi} \int_r^R \frac{dS(y)}{dy} (y^2 - r^2)^{-1/2} dy . \quad (9)$$

Abel transformations are widely applied for estimation of refractive index profile in the Earth atmosphere, also for research of bending of radio wave, sent by GPS satellite, in the atmosphere. Theoretically, the accuracy of the shadowgraphic method is limited only by the impact of diffraction in free-space propagation, which can be minimized by taking a small enough  $L$  or by backlighting the object with shorter-wavelength light.

### **High temporal resolution tomography of refractive index and absorption variation induced by light-plasma filaments**

In this part of the work, we study the variation of the refractive index change excited by light and plasma filament in water by means of time-resolved quantitative shadowgraphic method.

The experiment was carried out with an amplified Ti:sapphire laser system (SPITFIRE, Spectra Physics) delivering 800 nm, 120 fs pulses at 1 kHz rate. A spatially filtered laser pulse was loosely focused (beam waist diameter (FWHM) 109  $\mu\text{m}$ ) on the

front surface of a 20 mm long fused silica cell filled with deionized water to generate a filament of several millimeters. For a pulse energy of  $4 \pm 0.25 \mu\text{J}$ , the nonlinear focus was located at  $\sim 9.1$  mm beyond the input window of the cell. The changes in the refractive index induced by the filament were probed transversally by 560 nm, 23 fs (FWHM), spatially filtered pulses from a noncollinear optical parametric amplifier (TOPAS-White, Light Conversion Ltd.) pumped by the second harmonic of the laser. The probe pulses were delayed by a motorized time slide and negatively prechirped to compensate for the dispersion due to the water cell window and the propagation in water before reaching the plasma channel (2.5 mm). To record the shadowgraphs, we used a high spatial resolution imaging setup based on two 10 bit CCD cameras and imaging two parallel planes ( $P_0$  and  $P_1$ ) located inside the water cell. The plane  $P_0$  contains the filament, whereas the plane  $P_1$  is  $\sim 100 \mu\text{m}$  away from  $P_0$ . Both cameras were synchronized electronically and could grab single-shot images of the filament. The source term of the shadowgraphic equation was calculated by normalizing the difference of the two images from the intensity variation of the image of the plane  $P_1$ . This procedure was adopted to avoid systematic errors due to the absorption of the sample and reduce the impact of shot-to-shot fluctuations of the back-illuminating beam. The resolving power of the optical system was estimated experimentally to be  $\sim 1.5 \mu\text{m}$ . The refractive index maps are finally obtained by Abel inversion of the phase data retrieved from the shadowgrams. Figures 13(a) and 13(b) show a typical measurement of the filament track a few hundreds of micrometers beyond the nonlinear focus. The head of the filament is marked by a peak (dimensions FWHM  $5 \mu\text{m} \times 40$  fs) with positive variation of the refractive index (peak value  $\Delta n = +3 \times 10^{-4}$ ), followed by a narrow channel (average FWHM diameter  $5.5 \pm 1.5 \mu\text{m}$ ) with  $\Delta n = (-1.2 \pm 0.2) \times 10^{-4}$ . We attribute the positive index change to the optical Kerr effect, while the negative region is a clear signature of the existence of an electron plasma.

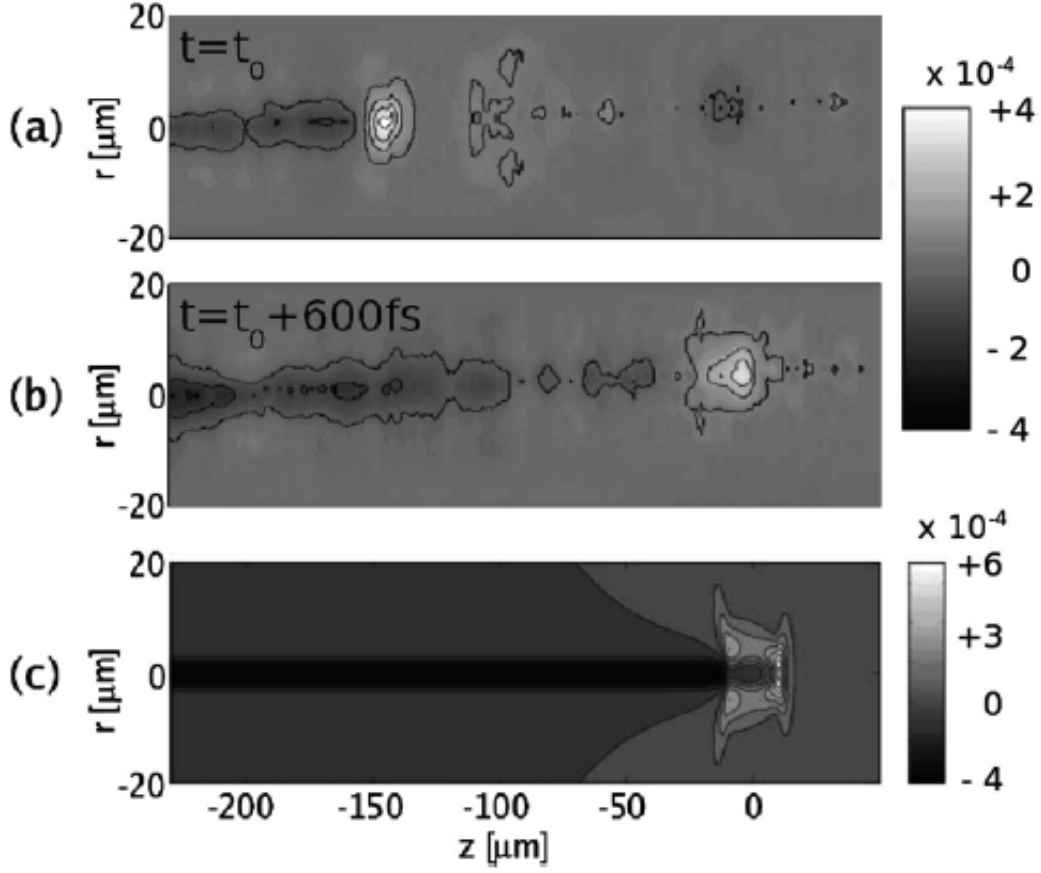


**Fig.13.** (a) and (b) Refractive index map of the filament taken at two different times and showing the formation of the plasma channel. Horizontal scale: propagation axis ranging from 9.41 mm (left) to 9.68 mm (right) from the input window. (c) Refractive index map obtained by numerical simulation of the experiment.

Assuming the refractive index of the plasma to follow the Drude model, the observation is consistent with an electron density of about  $n_e \approx (2.1 \pm 0.4) \times 10^{18} \text{ cm}^{-3}$ . The speed of the refractive index peak measured from our measurements at different probe delays was found to be  $0.2235 \pm 0.0005 \mu\text{m}/\text{fs}$  or  $(0.7455 \pm 0.0016)c$ , in agreement with the expected group velocity of light in water.

We compared our experimental data with numerical simulations [32]. Figure 13(c) shows the refractive index map obtained by simulation for input conditions as in the experiment. The set of parameters used in the model allowed us to reproduce with very good quantitative agreement the features of the filament visible on the map in Fig.13.

An inspection of the raw shadowgrams taken at the plane  $P_0$  provides useful information on the absorption of the probe pulse in the filament (see Fig.14). In

particular, we observe three features: (i) a strongly absorbing and localized head (corresponding to the peak of positive  $\Delta n$ ), followed by (ii) a zone with almost no absorption and (iii) a tail with slowly varying absorption (up to 3%). Figure 14(b) shows the on-axis transmittance of the probe pulse as a function of time at a given propagation distance from the input ( $z=9.52$  mm). We interpret the low transmittance of the head of the filament as the consequence of the simultaneous absorption of one photon of the probe ( $\lambda_1=560$  nm) and three photons of the pump beam ( $\lambda_0=800$  nm).

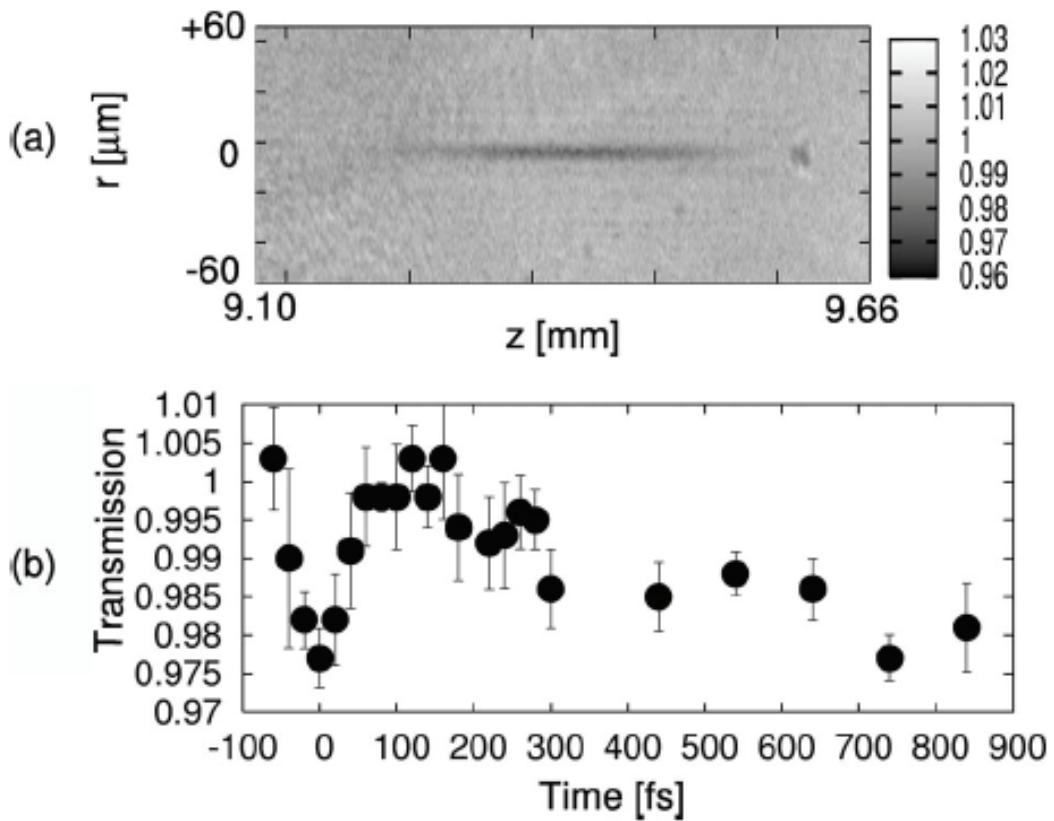


**Fig.14.** Absorption measurements of the filament at 560 nm as a function of (a) position for a given probing time and (b) time at position  $z=9.52$  mm. Error bars: 95% confidence.

Concerning the plasma channel in the wake of the pulse (buildup time of the absorption [ $\sim 0.5$ – $0.7$  ps] and very slow decay [ $\sim 90$  ps], as a possible explanation we propose to consider the role of the transient absorption induced by solvated electrons [33].

In conclusion, we have shown that quantitative shadowgraphy is a powerful tool for time-resolved refractometry of laser–plasma filaments in condensed media. This technique enabled us for the first time to take snapshots of the propagation of a femtosecond pulse in water and trace the dynamic of the formation of the plasma channel with a time resolution better than the pump pulse duration. Useful quantitative information such as the diameter (5.5  $\mu\text{m}$ ) and the electron density ( $n_e=2.1\times 10^{18}\text{ cm}^{-3}$ ) of the plasma channel generated by the writing pulse were deduced from the measured refractive index change and compared with the results of numerical simulations. Moreover, spatially resolved transient absorption measurements bear evidence of solvation effects of the electrons released during light–water interaction, providing useful insight into the chemical changes induced by femtosecond laser pulse propagation in water.

## 6 Conclusions

By means of high temporal (20 fs) and spatial (1  $\mu\text{m}$ ) resolution laser 3D mapping technique, it was shown that the initial Gaussian wave packet during self-action in Kerr media redistributes its energy in a way that in spatio-temporal domain the wave packet takes a complex X-type intensity distribution. This transformation is universal and is determined by temporal and spatial spectral broadening (as a consequence of self-focusing and self phase modulation), conical emission (as a consequence of four-wave mixing) and nonlinear losses caused by multiphoton absorption.

By means of imaging spectrometer technique it was shown that in the medium with normal group velocity dispersion the far-field angular spectrum of the wave packet takes a characteristic X shape, whereas in anomalous group velocity dispersion regime – a characteristic O shape. In both cases the localization of the wave packet is observed, however the quantitative differences of the angular spectra are determined by the phase-matching conditions of the four-wave mixing.

By means of high temporal (23 fs) and spatial (1,5  $\mu\text{m}$ ) resolution quantitative shadowgraphic method, free electron plasma induced by light filament in water was fully characterized. The dynamics of the refractive index along the filament core was investigated. It was found that the maximum local positive refractive index change of  $+3\times 10^{-4}$  is associated with the Kerr effect, whereas the negative refractive index change of  $-1.2\times 10^{-4}$  is associated with plasma defocusing. The measured negative refractive index change corresponds to  $2.1\times 10^{18}\text{cm}^{-3}$  free electron density in the plasma channel. The obtained data may help to estimate laser-induced long-term structural changes in the material and may be applied for fabrication of various microoptical elements in bulk media.

## 7 References

---

1. R.Y.Chiao, E. Garmire, C.H.Townes, Self-trapping of optical beams, *Phys. Rev. Lett.* **13**, 479 (1964).
2. M. Hercher, Laser-induced damage in transparent media, *J. Opt. Soc. Am.* **54**, 563 (1964).
3. W. Koechner. *Solid-state laser engineering*, - Springer-Verlag, Berlin, 1999.
4. A. Baltuska, T. Fuji, T. Kobayashi. Visible pulse compression to 4 fs by optical parametric amplification and programmable dispersion control, *Opt. Lett.* **27**, 306 (2002).
5. F. Courvoisier, V. Boutou, J. Kasparian, E. Salmon, G. Mejean, J. Yu, J.-P. Wolf, Ultraintense light filaments transmitted through clouds, *Appl. Phys. Lett.*, **83**, 213 (2003).
6. J. Kasparian, M. Rodriguez, G. Méjean, J. Yu, E. Salmon, H. Wille, R. Bourayou, S. Frey, Y.-B. André, A. Mysyrowicz, R. Sauerbrey, J.-P. Wolf, L. Wöste, White-Light Filaments for Atmospheric Analysis, *Science*, **301**, 61 (2003).
7. G. Cerullo, S. De Silvestri, Ultrafast optical parametric amplifiers, *Rev. Sci. Instrum.* **74**, 1 (2003).
8. D. Faccio, A. Averchi, A. Couairon, M. Kolesik, J. V. Moloney, A. Dubietis, G. Tamosauskas, P. Polesana, A. Piskarskas, and P. Di Trapani, Spatio-temporal reshaping and X Wave dynamics in optical filaments., *Opt. Express* **15**, 13077 (2007).
9. A. Zaïr, A. Guandalini, F. Schapper, M. Holler, J. Biegert, L. Gallmann, A. Couairon, M. Franco, A. Mysyrowicz, and U. Keller, Spatio-temporal characterization of few-cycle pulses obtained by filamentation, *Opt. Express* **15**, 5394 (2007).
10. S. Tzortzakis, B. Prade, M. Franco, A. Mysyrowicz, Femtosecond laser-guided electric discharge in air, *Phys. Rev. E*, **64**, 057401 (2001).
11. M. Châteauneuf, S. Payeur, J. Dubois, J.-C. Kieffer, Microwave guiding in air by a cylindrical filament array waveguide, *Appl. Phys. Lett.* **92**, 091104 (2008).
12. C. D'Amico, A. Houard, M. Franco, B. Prade, A. Mysyrowicz, A. Couairon, V. T. Tikhonchuk, Conical Forward THz Emission from Femtosecond-Laser-Beam Filamentation in Air, *Phys. Rev. Lett.* **98**, 235002 (2007).
13. D. Ashkenasi, H. Varel, A. Rosenfeld, S. Henz , J. Herrmann, E. E. B. Cambell, Application of self-focusing of ps laser pulses for three-dimensional microstructuring of transparent materials, *Appl. Phys. Lett.*, **71**, 1442 (1998).

- 
14. K. Yamada, W. Watanabe, Y. Li, K. Itoh, and J. Nishii, Multilevel phase-type diffractive lenses in silica glass induced by filamentation of femtosecond laser pulses, *Opt. Lett.* **29**, 1846 (2004).
  15. W. Watanabe, T. Asano, K. Yamada, K. Itoh, and J. Nishii, Wavelength division with three-dimensional couplers fabricated by filamentation of femtosecond laser pulses, *Opt. Lett.* **28**, 2491 (2003).
  16. H. Altug, D. Englund, J. Vučković, Ultrafast photonic crystal nanocavity laser, *Nature Physics*, **2**, 484 (2006).
  17. T. Wilhelm, J. Piel, and E. Riedle, Sub-20-fs pulses tunable across the visible from a blue-pumped single-pass noncollinear parametric converter, *Opt. Lett.* **22**, 1494 (1997).
  18. E. Garmire, R. Y. Chiao, C. H. Townes, Dynamics and characteristics of the self-trapping of intense light beams, *Phys. Rev. Lett.*, **16**, 347 (1966).
  19. S. A. Akhmanov, V. A. Vysloukh, A. S. Chirkin. *Optics of Femtosecond Laser Pulses*, - American Institute of Physics, New York, 1992.
  20. A. Braun, G. Korn, X. Liu, D. Du, J. Squier, and G. Mourou, Self-channeling of high-peak-power femtosecond laser pulses in air, *Opt. Lett.* **20**, 73 (1995).
  21. A. Dubietis, E. Gaižauskas, G. Tamošauskas, P. Di Trapani, Light filaments without self channelling, *Phys. Rev. Lett.* **92**, 253903 (2004).
  22. M. Mlejnek, E. M. Wright, and J. V. Moloney, Dynamic spatial replenishment of femtosecond pulses propagating in air, *Opt. Lett.* **23**, 382 (1998).
  23. M. Kolesik, E. Wright, and J. Moloney, Dynamic Nonlinear X Waves for Femtosecond Pulse Propagation in Water, *Phys. Rev. Lett.* **92**, 253901 (2004).
  24. H. Kumagai, S.-H. Cho, K. Ishikawa, K. Midorikawa, M. Fujimoto, S. Aoshima, Y. Tsuchiya, Observation of the complex propagation of a femtosecond laser pulse in a dispersive transparent bulk material, *J. Opt. Soc. Am. B* **20**, 597 (2003).
  25. Chen, Y. F., Beckwitt, K., Wise, F. W. and Malomed, B. A., Criteria for experimental observation of multi-dimensional optical solitons in saturable Kerr media, *Phys. Rev. E* **70**, 046610 (2004).
  26. A. Couairon and A. Mysyrowicz, Femtosecond filamentation in transparent media, *Phys. Rep.* **441**, 47 (2006).
  27. Q. Sun, H. Jiang, Y. Liu, Z. Wu, H. Yang, and Q. Gong, Measurement of the collision time of dense electronic plasma induced by a femtosecond laser in fused silica, *Opt. Lett.* **30**, 320 (2005).



- 
28. X. Mao, S. Mao, and R. E. Russo, Imaging femtosecond laser-induced electronic excitation in glass, *Appl. Phys. Lett.* **82**, 697 (2003).
  29. D. Faccio, A. Matijošius, A. Dubietis, R. Piskarskas, A. Varanavičius, E. Gaižauskas, A. Piskarskas, A. Couairon, P. Di Trapani, Near- and far-field evolution of laser pulse filaments in Kerr media, *Phys. Rev. E* **72**, 037601 (2005).
  30. A. Gopal, S. Minardi, and M. Tatarakis, Quantitative two-dimensional shadowgraphic method for high-sensitivity density measurement of under-critical laser plasmas, *Opt. Lett.* **32**, 1238 (2007).
  31. M. Kalal, K. A. Nugent, Abel inversion using fast Fourier transforms, *Appl. Opt.* **27**, 1956 (1988).
  32. A. Dubietis, A. Couairon, E. Kučinskas, G., Tamošauskas, E. Gaižauskas, D. Faccio, and P. Di Trapani, Measurement and calculation of nonlinear absorption associated with femtosecond filaments in water, *Appl. Phys. B* **84**, 439 (2006).
  33. R. Lian, R. A. Crowell, and I. A. Shkrob, Solvation and Thermalization of Electrons Generated by above-the-Gap (12.4 eV) Two-Photon Ionization of Liquid H<sub>2</sub>O and D<sub>2</sub>O, *J. Phys. Chem. A* **109**, 1510 (2005).

## Santrauka

Šviesos netiesinio fokusavimosi reiškinys tyrinėjamas jau nuo pat lazerio sukūrimo. Ypatingai aktyviai nagrinėjamas šviesos gijų susidarymas bei jų dinamika skirtingos fazinės būsenos medžiagose. Šviesos gijos įdomios tuo, kad šviesa jose sklinda beveik nepatirdama difrakcijos ir dispersijos. Mokslininkai pasiūlė nemažai šviesos gijos taikymų, kaip pvz. atmosferos sluoksnių spektrinė analizė, atosekundinių impulsų generacija inertinėse dujose ar bangolaidžių užrašymas kietose skaidriose terpėse. Šviesos saviveikos metu pradinė bangų paketų forma erdvėje bei laike gali stipriai pakisti. Standartiniai impulsų charakterizavimo metodai, kurie remiasi erdvėje integruotų autokoreliacinių ir kryžminių koreliacinių funkcijų matavimu, įgalina gauti tik dalinę informaciją apie vykstančias šviesos impulso bei terpės savybių transformacijas ir jų fizikinę prigimtį. Todėl, norint gerai įvaldyti minėtus taikymus bei suprasti vykstančius fizikinius reiškinius, visiškam šviesos impulsų sąveikos su medžiaga ir šviesos gijų formavimo proceso charakterizavimui reikalingi nauji matavimo metodai, kuriuos pasitelkus būtų galima išmatuoti bangų paketo intensyvumo pasiskirstymą trijų matmenų erdvėje bet kuriuo laiko momentu bei registruoti momentinius terpės struktūros pokyčius. Antra vertus, šviesos ir medžiagos sąveikos procesai yra labai spartūs, tad jų tyrimui reikalinga labai didelė tiek erdvinė ( $\mu\text{m}$  eilės), tiek laikinė ( $\text{fs}$  eilės) skyra.

Šiame darbe pasiūlėme didelės laikinės (20 fs) ir erdvinės (1  $\mu\text{m}$ ) skyros lazerinės tomografijos metodiką, kuria rementis, parodyta, kad pradinio Gauso formos bangų paketo energija saviveikos Kero terpėje metu persiskirsto taip, kad erdvėlaikyje jis įgauna sudėtingą X tipo intensyvumo skirstinį. Ši transformacija yra universali, ir ją nulemia laikinis ir erdvinis spektro plitimas (dėl fokusavimosi ir fazės moduliavimosi), kūginė spinduliuotė (dėl keturbangio maišymosi) bei nuostoliai dėl daugiafotonės sugerties.

Taip pat pasiūlėme impulsų kampinių spektrinių skirstinių registravimui naudoti atvaizduojančio spektrometro metodiką, kuria remiantis, parodyta, kad normalios grupinių greičių dispersijos terpėje bangų paketo tolimojo lauko kampinis spektrinis skirstinys yra X formos, o anomalios grupinių greičių dispersijos terpės atveju – O formos. Abiem atvejais stebima bangų paketo lokalizacija, tačiau kiekybinius kampinių

spektrinių skirstinių skirtumus nulemia keturbangio dažnių maišymo fazinio sinchronizmo sąlygos.

Ir galiausiai, naudojant didelės laikinės (23 fs) ir erdvinės (1,5  $\mu\text{m}$ ) skyros kiekybinį šešėlinį metodą, pilnai charakterizuotas šviesos gijos inicijuotas laisvųjų elektronų plazmos kanalas vandenyje. Ištirta lūžio rodiklio dinamika išilgai šviesos gijos ir nustatyta, kad lokalus teigiamas lūžio rodiklio pokytis, susijęs su Kero efektu, siekė  $+3,0 \times 10^{-4}$ , tuo tarpu neigiamas lūžio rodiklio pokytis, susijęs su plazmos defokusavimu, siekė  $-1,2 \times 10^{-4}$ , kuris atitinka  $2,1 \times 10^{18} \text{ cm}^{-3}$  laisvųjų elektronų tankį plazmos kanale. Gauti duomenys leistų prognozuoti ilgai gyvuojančių struktūrinių medžiagos pokyčių inicijavimą lazeriu ir būti pritaikyti įvairių mikrooptinių elementų formavimui plačios apertūros kristaluose.

## **Brief information about the author**

Name: Rimtautas

Surname: Piskarskas

Date and place of birth: June 29, 1979, Vilnius, Lithuania

Email: rimtautas.piskarskas@ff.vu.lt

Professional experience:

1998: Graduated Vilnius Liceum

2002: Bachelor degree, Vilnius University, Faculty of Physics

2002.10 – 2003.03: Practice in Laser Centre Hannover, Germany

2004: Master degree, Vilnius University, Faculty of Physics

2004-2008: PhD studies, Vilnius University, Department of Quantum Electronics.

2006.05: Practice in Insubria University, Como, Italy

2007.02: Practice in University of Pavia, Pavia, Italy

2007.06: Practice in STELLA Summer School, Vilnius, Lithuania

2007.08: Practice in OLA Summer School, Chania, Greece